Chapter: IV

Emergence of a New Modulated Phase and Ferromagnetism in Nanocrystalline $Nd_{0.5}Sr_{0.5}MnO_3$ Ceramic

Chapter-IV

4.1 Introduction

In previous chapter, we have discussed for several half doped nanocrystalline manganites that the low temperature charge ordering transition is suppressed when crystallite size is decreased to nanometer sizes [Shankar et al. (2015); Giri et al. (2011); Rao et al. (2006); Rao et al. (2005); Jirak et al. (2010); Shankar et al. (2015)]. In this chapter, we will discuss the crystallite size dependent changes in magnetic behavior and crystal structure of nanocrystalline $Nd_{0.5}Sr_{0.}5MnO_3$. As discussed in section 1.9.4 of chapter I, the structural and magnetic aspects of bulk $Nd_{0.5}Sr_{0.5}MnO_3$ (NSMO) has been investigated extensively by earlier authors. It is reported for the bulk samples of $Nd_{0.5}Sr_{0.5}MnO_3$ that during transition from high temperature ferromagnetic metallic to low temperature antiferromagnetic insulating charge ordered state, the crystal symmetry is lowered to monoclinic $P2_1/m$ [Kuwahara et al. (1998); Eremenko et al. (2001)]. Ritter et al [Ritter et al. (2000)] reported that the lower temperature antiferromagnetic insulating charge ordered phase is phase segregated into two different crystallographic structures and three magnetic phases, orthorhombic (*Imma*) ferromagnetic, orthorhombic (*Imma*) antiferromagnetic and monoclinic ($P2_1/m$) charge ordered CE type antiferromagnetic.

Although the crystal structure, magnetic properties and charge ordering are well studied in the cases of bulk NSMO manganites [Kawano et al. (1997); Urushibara et al. (1995); Kajimoto et al. (2002)], such a phenomena is not explored much in the nanocrystalline forms. Recent studies in this direction have revealed that the reduction

of the particle size has strong influence on charge ordering and magnetic transition in NSMO [Biswas et al. (2005); Biswas et al. (2006); Rao et al. (2005); Biswas et al. (2007); Laffez et al. (1996); Kundu et al. (2012)]. The nano samples of the half doped LCMO, NCMO and PCMO manganites investigated in previous chapter exhibit same crystal structure as the bulk one [Shankar et al. (2015)]. In this chapter, we show that a new modulated monoclinic crystal structure is observed for the nanocrystalline $Nd_{0.5}Sr_{0.5}MnO_3$ (NSMO) ceramic, which is completely different from the structure of bulk sample. This new crystalline phase of nano NSMO sample is expected to offer new functionalities for various device applications. In contrast to the bulk sample, the nanocrystalline samples retain the ferromagnetic state down to low temperatures and charge ordering transition is absent.

4.2 Experimental and Characterization Details

As discussed in chapter II, the dark brown precursor powder of NSMO was prepared by combustion synthesis. This powder was divided into several parts and calcined at 600, 700, 800, 900, 1000, 1100 1200 and 1300^{o}C for 6 hours to obtain samples of various crystallite sizes. The samples calcined at these temperatures will be denoted by C6, C7, C8, C9, C10, C11, C12 and C13 respectively in the following sections. Same precursor was used to prepare samples of various crystallite sizes so that stoichiometry is same in all the samples. We have reported recently that this synthesis method gives very good quality of manganite samples [Shankar et al. (2015)]. As shown in sections 4.3.2, the magnetic transition temperatures of our bulk sample matches well with those reported in literature attesting good quality of the samples. The

crystallite/particle sizes of the samples were determined by Scherrer formula, Scanning electron microscopy and Rietveld method. The structural and magnetic characterization of the samples revealed that the samples calcined at temperatures ≥1000 ^{O}C behave as bulk while those calcined at lower temperatures exhibit nano features. The crystallite size for the samples calcined at 600 ^{O}C, 900 ^{O}C and 1300 ^{O}C was obtained to be ~16.3 nm, 89.45 nm and 0.45 μm respectively.

4.3 Results and Discussion

4.3.1 Microstructural and Spectroscopic Analysis of the Samples

Before the crystal structure and magnetic studies, to check the quality of the samples, we characterized the microstructure, composition and Mn^{4+}/Mn^{3+} ratio by SEM, TEM, EDS and XPS measurements respectively. Fig. 4.1(a) shows the SEM image of the bulk sample calcined at 1300 ^{o}C. As can be seen from Fig. 4.1(a), the bulk sample exhibits uniform dense microstructure with average grain size ~0.45μm. The microstructure of the nanocrystalline NSMO sample (calcined at 900 ^{o}C) shown in Fig.4.1(c) exhibits uniform grains with average size ~49.9 (2) nm. Inset to Fig. 4.1(d) show the TEM image of the nanocrystalline NSMO sample (calcined at 900 ^{o}C). The average grain size from TEM studies also comes to ~48.3(3) nm. The crystallite size for this sample determined by Rietveld analysis is ~52.2 (3) nm which is in well agreement with the microscopic results. We also calculated the crystallite size of NSMO samples obtained at various calcination temperatures using Rietveld analysis.

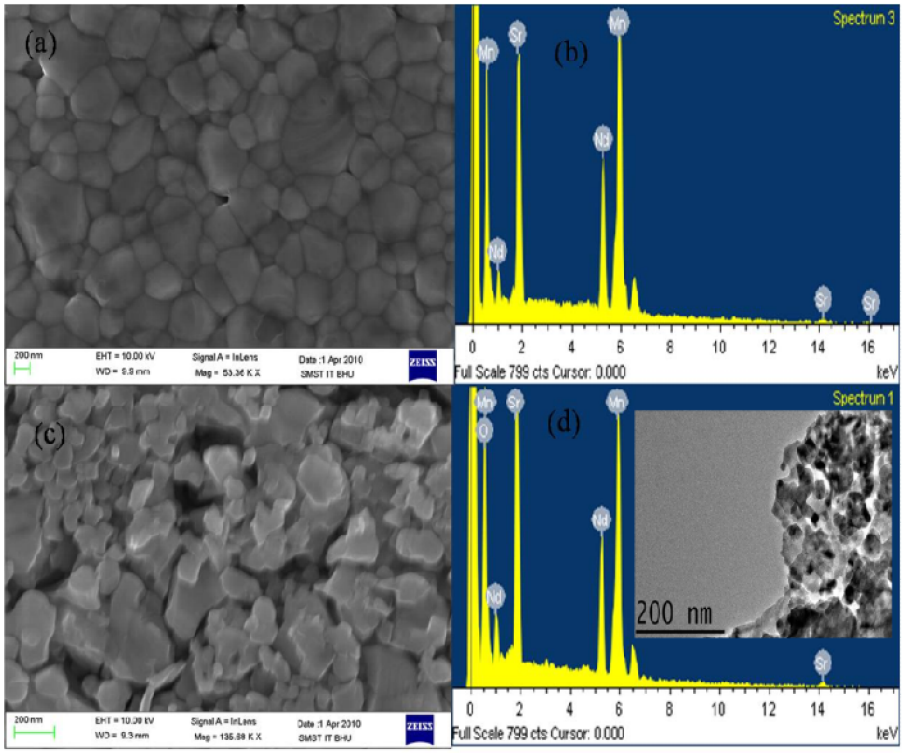

Fig. 4.1. Scanning electron microscopic (SEM) images of (a) bulk (C13) and (c) nano (C9) $Nd_{0.5}Sr_{0.5}MnO_3$ samples. Energy dispersive Spectrum (EDS) of samples (b) C13 and (d) C9. Inset to Fig. 4.1(d) shows the TEM image of C9 sample.

The crystallite sizes for the calcination temperatures 600, 700, 800, 900, 1000, 1100, 1200 and 1300 ^{o}C were obtained to be ~16.2 (1), 38.9 (2), 44.6 (4), 49.9 (2), 90.1 (7), 340 (3), 420 (1) and 450 (4) nm respectively. Fig. 4.1(b, d) show the EDS spectrum for the nanocrystalline (C9) and bulk (C13) samples. The nominal composition atomic percentage of Sr, Mn, Nd and O in $Nd_{0.5}Sr_{0.5}MnO_3$ corresponds to 10, 20, 10 and 60% respectively. The experimentally calculated atomic percentages for nanocrystalline and bulk samples were found to be in well agreement with the nominal composition within the experimental error.

Fig. 4.2 shows the XPS spectrum of Mn corresponding to the $2p_{3/2}$ electron for the nanocrystalline and bulk NSMO samples calcined at 600 ^{o}C and 1300 ^{o}C respectively. In manganite samples, the binding energy of the Mn $2p_{3/2}$ electron for the Mn^{4+} ion is reported to be ~642.4 eV while that for the Mn^{3+} ion ~640.7 eV [Symianakis et al. (2015)]. In nanocrystalline NSMO sample, analysis of the XPS spectrum gives the binding energy of the Mn $2p_{3/2}$ electron as ~642.4 eV for the Mn^{4+} ion while that for the Mn^{3+} ion as ~640.7 eV. For bulk NSMO sample the binding energy of the Mn $2p_{3/2}$ electron for the Mn^{4+} ion is obtained to be ~642.18 eV while that for the Mn^{3+} ion, it is ~640.6 eV. We fitted the XPS spectrum by two peaks at these positions for the Mn^{4+} and Mn^{3+} ions and calculated their relative fraction using the area under peaks. This gives equal proportion of the Mn^{+4} and Mn^{+3} ions for both the bulk and nanocrystalline samples. In doped rare earth perovskite manganites, presence of oxygen nonstoichiometry is known to affect the valance state and relative proportion of the Mn ions so that electroneutrality is maintained. An oxygen rich sample is expected to have higher Mn^{4+}/Mn^{3+} ratio than the nominal composition.

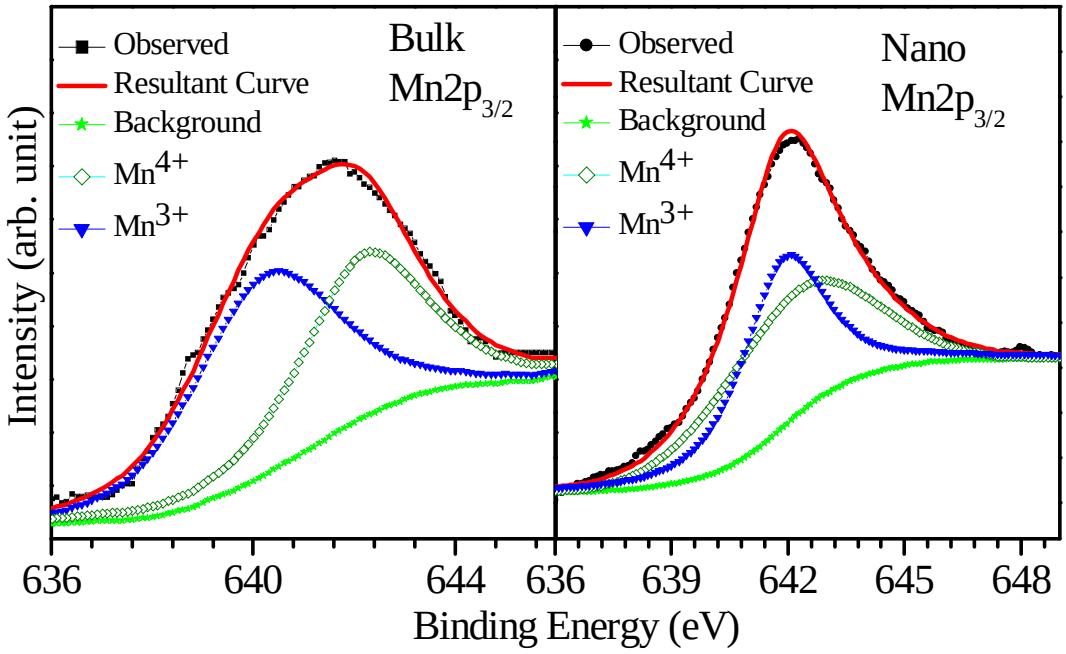

Fig. 4.2. X-ray photoelectron spectra (solid circles) of Mn $2p_{3/2}$ core level for bulk (C13) and nano (C6) $Nd_{0.5}Sr_{0.5}MnO_3$. The solid triangles and solid squares show the core level peak fits for the Mn^{4+} and Mn^{3+} ions, respectively. The bottom curve (stars) shows Shirley background. The continuous line overlapping the observed XPS data (solid circles) shows the resulting curve fit.

The oxygen deficient sample will have lower value of the Mn^{4+}/Mn^{3+} ratio than the nominal composition. As per the nominal composition of $Nd_{0.5}Sr_{0.5}MnO_3$ the Mn^{4+}/Mn^{3+} ratio should be one which is experimentally obtained for both the bulk and nano NSMO samples. This result confirms that our samples are of good quality and have stoichiometric oxygen content.

4.3.2 Magnetic Phase Transitions in Nanocrystalline and Bulk NSMO Samples

To investigate the magnetic phase transition behavior of bulk and nano NSMO samples M-T measurements on C6, C9 and C13 samples were done. The magnetization vs. temperature (M-T) measurement plots at 0.05T field strength for the bulk (C13) and nanocrystalline (C6 and C9) $Nd_{0.5}Sr_{0.5}MnO_3$ samples are shown in Fig.4.3 (a, b, c). The measurements were done under zero-field cooling (ZFC), field-cooled cooling (FCC) and field-cooled warming (FCW) runs for the C6 and C9 samples while ZFC and FCW runs for bulk sample. The FCW and FCC data are superimposed on each other for both the C6 and C9 sample which indicates that there is no glassy contribution in the system. The nature of the temperature dependent magnetization curves in the temperature range 5K-300K are seen to be very different from one another for the nanocrystalline and bulk samples.

For bulk sample, it can be seen from Fig. 4.3(a) that with decreasing temperature the magnetization takes increasing trend due to transition from room temperature paramagnetic phase to lower temperature ferromagnetic phase.

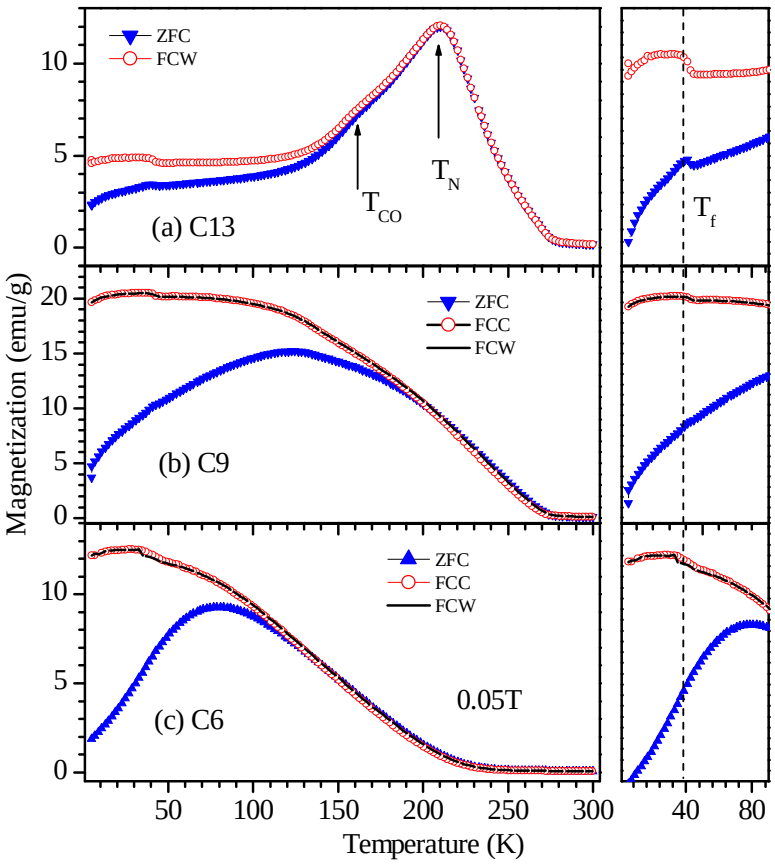

Fig. 4.3. Magnetization vs temperature (M-T) plots for the samples (a) bulk (C13), (b) nano (C9), (c) nano (C6) measured at the magnetic field of 0.05 T. Zoomed portion of the M-T plot at lower temperatures.

The M-T curve shows a peak around ~ 225 K and then magnetization decreases due to ferromagnetic to antiferromagnetic phase transition. The ferromagnetic to antiferromagnetic transition temperature (T_N~225K) is in well agreement with the earlier reports [Yu et al. (2005)]. The M-T curve shows another weak anomaly around the temperature 160K which corresponds to charge ordering transition [Kuwahara et al. (1995); Lopez et al. (2002)].The paramagnetic to ferromagnetic transition temperature (T_C ~ 250K) and charge ordering transition temperatures (T_{CO} ~160K) are not clearly distinct in the M-T curve. We show in the right panel of Fig.4.3 (a, b, c), the zoomed portion of the M-T plot at lower temperatures. As can be seen from this figure the M-T plot of all the three samples (C6, C9 and C13) show an anomaly around 40K. This anomaly corresponds to another transition involving the formation of FM clusters in antiferromagnetic matrix. Similar behaviour is reported in $La_{0.75}Ca_{0.25}MnO_3$ also [Fernandez-Martinez et al. (2014)]. The temperature dependences of dc χ^{-1} at 0.05 T magnetic field in ZFC measurement for bulk sample C13 is shown in Fig.4.4 (a). The paramagnetic to ferromagnetic transition temperature as determined form the Curie-Weiss fit for bulk sample comes out to be ~250K. Fig. 4.4(d) shows the dM/dT vs. T plot. The transition temperatures T_N and T_{CO} are very clearly seen in this figure and are marked with arrow. The values of the T_C (~250K), T_N (~225K) and T_{CO} (~160K) for the bulk sample are in well agreement with the earlier reports [Yu et al. (2005)]. The M-T curves for the nanocrystalline samples shown in Fig.4.3 (b, c) reveal only one transition from paramagnetic to ferromagnetic phase. In the FCC and FCW measurements, the magnetization does not show any downward trend at lower temperatures suggesting absence of antiferromagnetic transition in these samples.

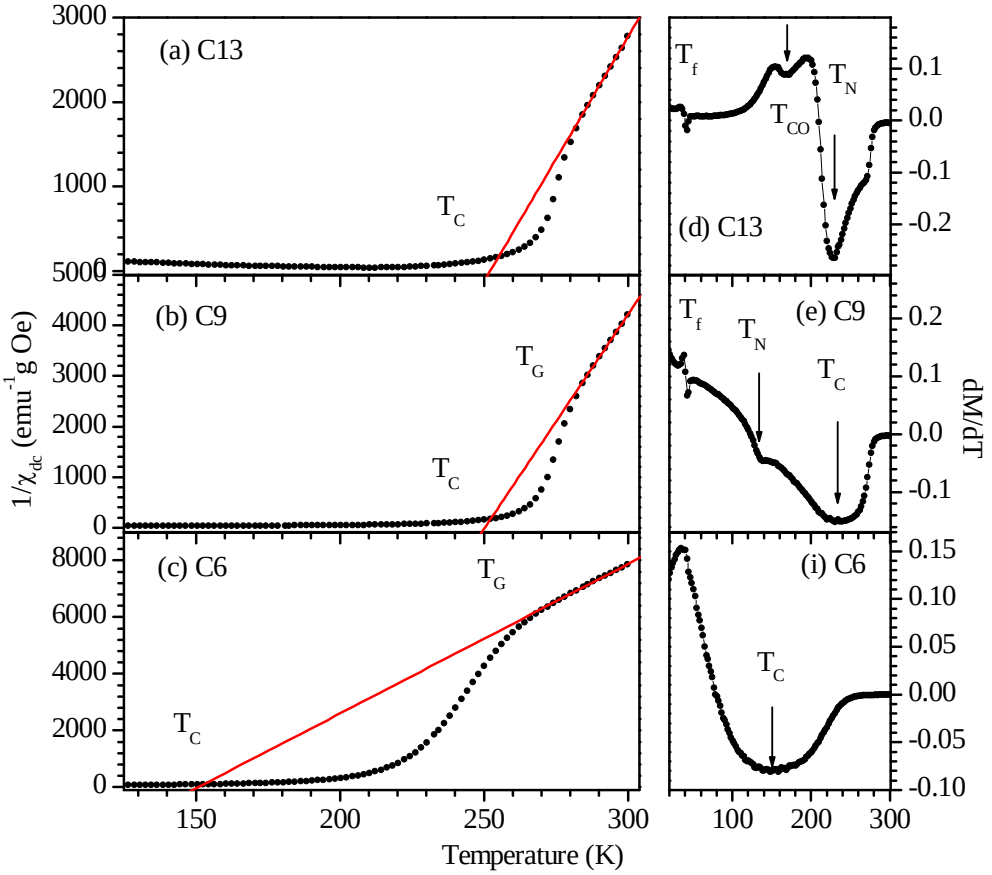

Fig. 4.4. The inverse susceptibility (χ^{-1}) vs Temperature (T) plots of the samples (a) C13, (b) C9, (c) C6 and first derivative of magnetization (dM/dT) vs temperature (T)) of the samples (d) C13, (e) C9, (f) C6 $Nd_{0.5}Sr_{0.5}MnO_3$ ceramic.

The temperature dependences of dc χ^{-1} at magnetic field 0.05 T, derived from the ZFC-M(T) curves for the C6 and C9 samples are shown in Fig. 4.4(b) and Fig. 4.4(c). The paramagnetic to ferromagnetic transition temperatures (T_C) determined form the Curie-Weiss fit for C6 and C9 samples comes out to be ~150 K and ~245 K respectively. This suggests that T_C is significantly shifted to lower temperature side for the nanocrystalline sample prepared at 600 ^oC. This is in contrast to the $La_{0.5}Ca_{0.5}MnO_3$ where T_C increases with decreasing crystallite size in nanocrystalline samples [Jirak et al. (2010)]. The dM/dT *vs* T curve for the C6 and C9 samples are shown in Fig.4.4 (e, f). It can be clearly seen that C9 sample shows a shallow minimum in addition to a deep minimum where M-T curve changes the slope. The minima around 245 K is identified as due to T_C as determined from the Curie-Weiss fit of the χ^{-1} *vs* T plot. The shallow minimum around 140 K may correspond to T_{CO} which is slightly on the lower temperature side in comparison to the bulk sample. Both the T_C (~245 K) and T_{CO} (~140 K) are shifted to the lower temperatures for C9 sample in comparison to the bulk sample and a broad minimum is seen around T_C. For the C6 sample calcined at 600 ^oC, only one minimum corresponding to T_C (150 K) is seen in dM/dT *vs* T curve. There is no signature of charge ordering transition in this sample. In addition, a careful examination of the χ^{-1} vs T plots shown in Fig.4.4 (b, c) suggests that there are two linear slopes in the paramagnetic region. Such a variation of χ^{-1} in the paramagnetic region is considered as the characteristics of Griffith's singularity in nanocrystalline samples [Salamon et al. (2003)]. The Griffiths phase was first proposed by Griffiths [Griffiths (1969)] to explain the effects of the quenched randomness on the magnetization of a dilute Ising ferromagnet.

The Griffiths phase means the existence of short-range ordering of ferromagnetic clusters in a paramagnetic matrix when $T_C \leq T \leq T_G$. A Griffiths Phase (GP) like behavior clearly exists below the critical temperature (T_G) where magnetization shows a downturn. The onset of this downturn is denoted as T_G below which the ferromagnetic cluster emerges in the paramagnetic matrix. The values of T_G for the C6 and C9 samples are found to be ~260 K and ~280 K respectively. A weak signature of T_G around 282K is seen in bulk sample also. This may due the fact that our bulk sample is also having average grain size ~0.5 μm and some smaller grains can contribute to Griffith's singularity. The Magnetization (M)-applied magnetic field (H) curves of the bulk and nanocrystalline (C6 and C9) NSMO at 5 K are shown in Fig. 4.5. The nanocrystalline samples exhibit clearly open M-H curve characteristic of ferromagnetic state. The experimentally calculated magnetizations per formula unit for C6, C9 and C13 samples are 1.28μB, 2μB and 1.00μB respectively. The theoretically calculated magnetization per formula unit is 3.5μB. This suggests that the fraction of the sample in ferromagnetic state for C6, C9 and C13 are 36.57%, 57.14% and 28.57% respectively. The sample calcined at 900 ^oC is having significantly larger magnetization than that for the 600 ^oC. This is attributed to the increased spin disorder at the surface in smaller crystallite size sample. In contrast, the bulk sample show very slim loop due to contributions from small coexisting ferromagnetic phase along with the low temperature antiferromagnetic phase as reported by earlier authors also [Lopez et al. (2002)]. The calculated phase fraction of the room temperature Imma phase at 13K is ~33.76%.

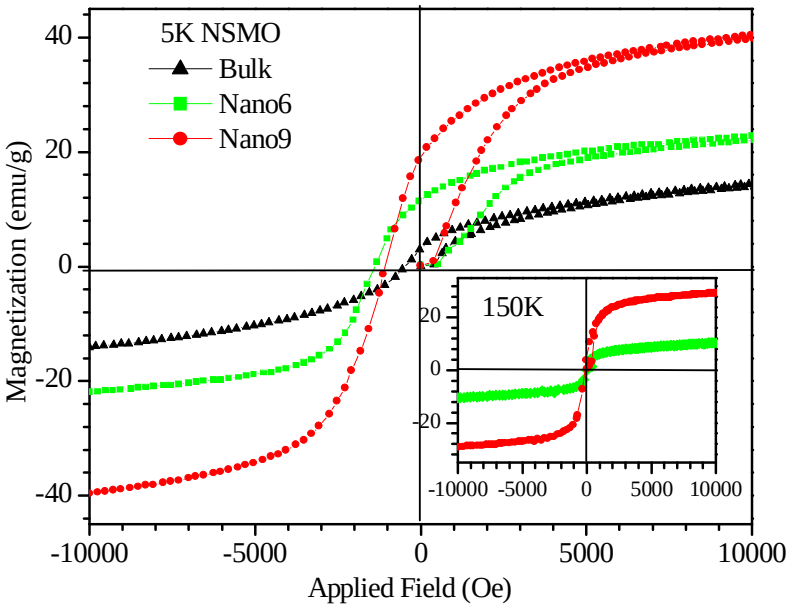

Fig. 4.5. The Magnetization (M) vs applied magnetic field (H) plot for bulk and nanocrystalline $Nd_{0.5}Sr_{0.5}MnO_3$ at 5 K (main panel) and at 150 K (inset). Hysteresis indicative of ferromagnetism is clearly seen at 5 K. Inset also shows the ferromagnetic behaviour for both the samples.

If we assume that this phase retains the ferromagnetic character then the fraction of the ferromagnetic phase (~28.57%) calculated from the M-H loop of the bulk samples is in well agreement. The inset to Fig 4.5 shows the M-H curve for nano samples (C6 and C9) recorded at 150 K. The hysteresis loops show ferromagnetic character but the magnetization is significantly reduced due to the temperature close to the T_C. All the three samples show paramagnetic behavior at room temperature.

4.3.3 Structural Phase Transitions in Bulk NSMO Sample

Fig. 4.6 shows the x-ray diffraction (XRD) patterns of $Nd_{0.5}Sr_{0.5}MnO_3$ samples calcined at various temperatures in the temperature range 600^{o}C to 1300^{o}C at 100 ^{o}C intervals. Earlier authors have reported the structure of the bulk NSMO sample (C13) to be orthorhombic but there is controversy about the space group in the existing literature. A group of authors have reported *Pnma* space group [Moritomo et al. (1997)] while many authors have reported *Imma* space group [Eremenko et al. (2001); Kundu et al. (2012); Woodward et al. (1999)]. To determine the correct space group, we analyzed the XRD pattern of C13 sample using both the space groups by Rietveld structure refinement. In *Pnma* space group many additional superlattice reflections appear in addition to those observed for the Imma space group The observed superlattice reflection satisfy the reflection conditions hkl: h+k+l = 2n and hk0: h = 2n for *Imma* symmetry as reported by Caignart et al [Caignart et al. (1996)] also. Rietveld structural analysis of the XRD data for C13 using both the space groups by us suggests that the correct space group is *Imma* as there are no superlattice reflections corresponding to the *Pnma* space group.

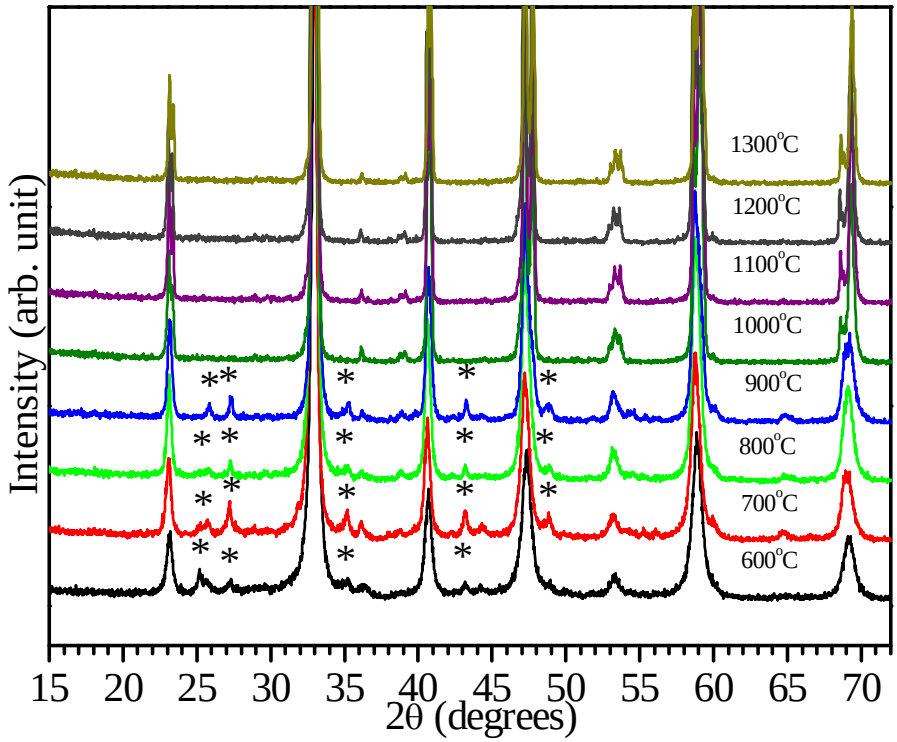

Fig. 4.6. Powder XRD patterns of $Nd_{0.5}Sr_{0.5}MnO_3$ ceramics prepared at various calcination temperatures 600 °C, 700 °C, 800 °C, 900 °C, 1000 °C, 1100 °C, 1200 °C and 1300 °C. The strong superstructure peaks are marked by asterisks.

This is in agreement with the reports of woodward et al [Woodward et al. (1999)], a prominent superlattice reflection (111) is expected around the two theta position 25.90 for the *Pnma* space group. It is not seen in the experimental XRD data of our bulk sample C13. A very good fit between observed and calculated XRD profiles using *Imma* space group is shown in Fig. 4.7. The refined cell parameters for the bulk sample C13 using *Imma* space group are a_o=5.4688 (2) Å, b_o=7.6231 (1) Å, and c_o=5.4286 (1) Å which matches well with the reported bulk lattice parameters by earlier authors [Eremenko et al. (2001); Kundu et al. (2012)]. A comparison of the XRD patterns of the samples calcined at various temperatures with that for the bulk sample C13 suggests that several new weak reflections (marked with asterisks) appear for the samples calcined below 1000 ^{0}C when crystallite size is in the nanocrystalline range (see Fig.4.6). Before we discuss the structure of these nanocrystalline samples, we will present the results of structural and phase transitions studies on bulk sample C13 calcined at 1300^{o}C to have a comparison between structure and phase transitions in nanocrystalline samples with the bulk one.

Fig.4.8 depicts the evolution of powder x-ray diffraction profiles of orthorhombic (101/020), (002/200/121), (202/040) and (004/400/242) reflections with temperature for the bulk $Nd_{0.5}Sr_{0.5}MnO_3$ sample at various temperatures in the temperature range 13 K to 300 K recorded in the heating run. The low temperature structure of the bulk NSMO is reported to be coexistence of the room temperature orthorhombic (*Imma*) and lower temperature monoclinic structures in the $P2_1/m$ space group which results from the charge ordering of Mn^{4+} and Mn^{3+} ions at B-site in the ABO_3 perovskite structure [Woodward et al. (1999)].

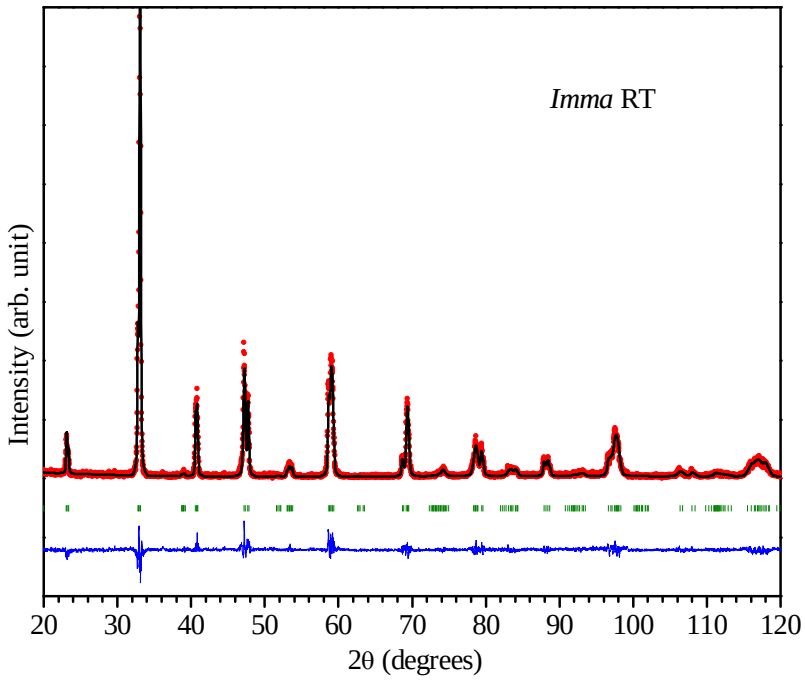

Fig. 4.7. Experimentally observed (dots), Rietveld calculated (continuous line) and their difference (continuous bottom line) profiles for bulk(C13) $Nd_{0.5}Sr_{0.5}MnO_3$ at 300K obtained by using *Imma*. The vertical tick marks above difference plot show the Bragg peak positions.

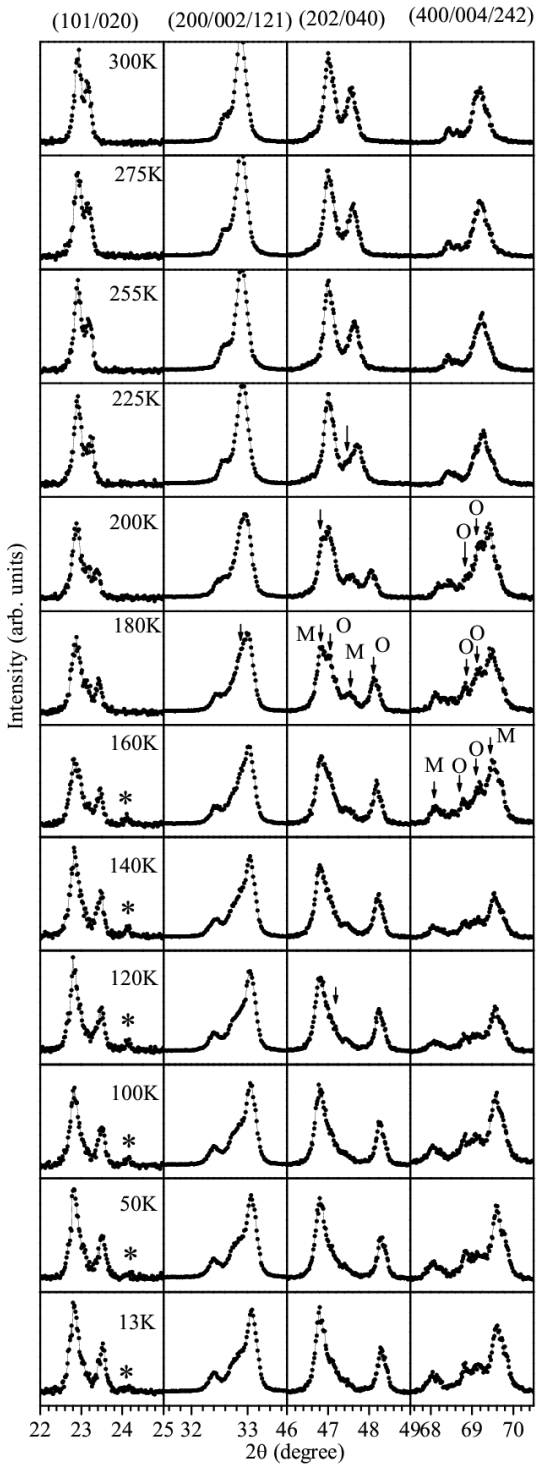

Fig. 4.8. Evolution of selected XRD profiles with temperature (13 K to 300 K) for bulk (C13) $Nd_{0.5}Sr_{0.5}MnO_3$ sample. The miller indices on top correspond to indexing using orthorhombic structure.

A comparison of the XRD profiles at 300K with that at 13K suggests that in addition to the XRD profiles corresponding to the high temperature orthorhombic (*Imma*) phase, many new reflections corresponding to the charge ordered monoclinic phase are also present at 13 K. The clear evidence for the low temperature monoclinic $P2_1/m$ phase is seen in the appearance of a super lattice reflection around two-theta =24.2 marked with asterisk. The 202/040 XRD profile at room temperature is doublet in the orthorhombic phase. Cooling down to lower temperatures makes it quadruplet at the temperatures 200K and 180K due to appearance of coexisting monoclinic phase. The peak profiles corresponding to the room temperature orthorhombic phase also show increased splitting due to increased orthorhombic distortion at lower temperatures. In the phase coexistence region (T<225 K) the peaks corresponding to monoclinic and orthorhombic structures are marked with letters M and O respectively for the patterns where they are well resolved. The room temperature (200/121) orthorhombic profiles exhibit significant broadening at lower temperatures due to presence of additional overlapping reflections corresponding to the coexisting monoclinic phase. The XRD patterns from room temperature to 225 K show only triplet nature for (400/040/242) profiles corresponding to the orthorhombic structure. On further cooling to lower temperatures, multiple reflections are observed which again confirms the coexistence of orthorhombic and monoclinic phases at lower temperatures. The intensity of the peaks corresponding to the charge ordered monoclinic phase decreases with increasing measurement temperature. The superlattice peak corresponding to the charged ordered monoclinic phase persists up to the temperature 160 K above which it is not clearly seen.

As revealed from the magnetic measurements shown in Fig.4.3, the charge ordering transition in bulk NSMO occurs around 160K. Thus the appearance of the super lattice reflection in the XRD pattern and charge ordering transition temperature (T_{CO}) are in well agreement for the bulk sample. A careful inspection of the 202/040 XRD profiles suggest that the low temperature monoclinic phase persist upto 200 K and disappears for the temperature above 225 K. Coexistence of the monoclinic and orthorhombic phases in wide temperature range across the transition temperature suggests first order nature of the phase transition in the crystal structure. The crystal structure of the bulk $Nd_{0.5}Sr_{0.5}MnO_3$ were analyzed by Rietveld structural analysis considering room temperature orthorhombic (*Imma*) space group for the patterns above 225 K while coexistence of orthorhombic (*Imma*) and monoclinic ($P2_1/m$) structures for lower temperatures. The Rietveld fits of XRD data using coexisting orthorhombic and monoclinic phases in *Imma* and $P2_1/m$ space groups at 13 K is shown in Fig.4.9. Very good fit between observed and calculated XRD profiles is obtained. The refined structural parameters and various agreement factors for orthorhombic and monoclinic structures are given in table 4.1 and 4.2. The calculated phase fractions of the monoclinic and orthorhombic phases are 66.24% and 33.76% respectively at 13 K.

The evolution of temperature dependent lattice parameters and unit cell volume of bulk NSMO (C13) for various crystallographic phases are shown in Fig.4.10, compare this variation with literature [Woodward et al. (1999)]. The orthorhombic and monoclinic lattice parameters show insignificant change in the two phase region at lower temperatures except slight thermal contraction. The c-lattice parameter is nearly temperature independent in the investigated temperature range from 300 K to 13 K.

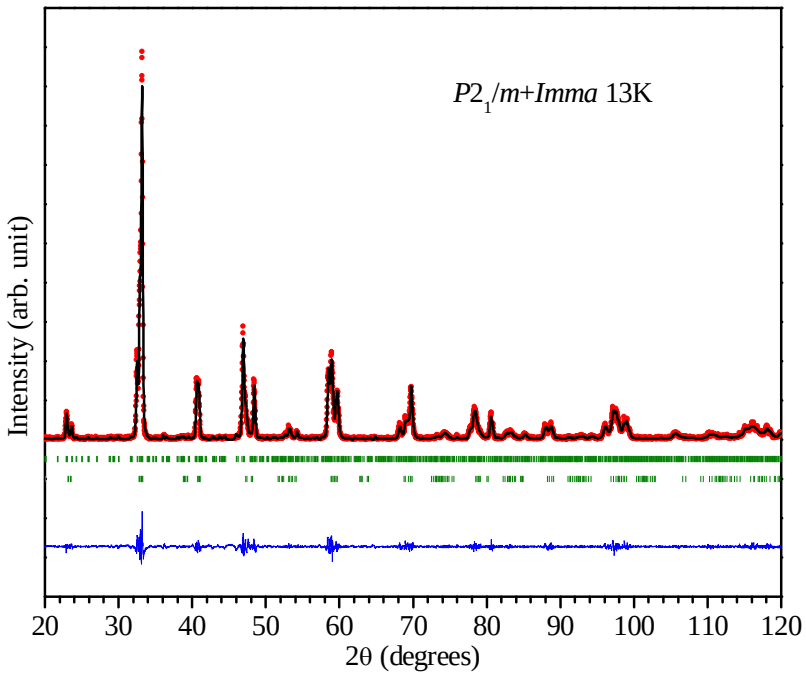

Fig. 4.9. Experimentally observed (dots), Rietveld calculated (continuous line) and their difference (continuous bottom line) profiles for bulk(C13) $Nd_{0.5}Sr_{0.5}MnO_3$ at 13K obtained by using coexisting *Imma*+$P2_1/m$ space groups. The vertical tick marks above difference plot show the Bragg peak positions.

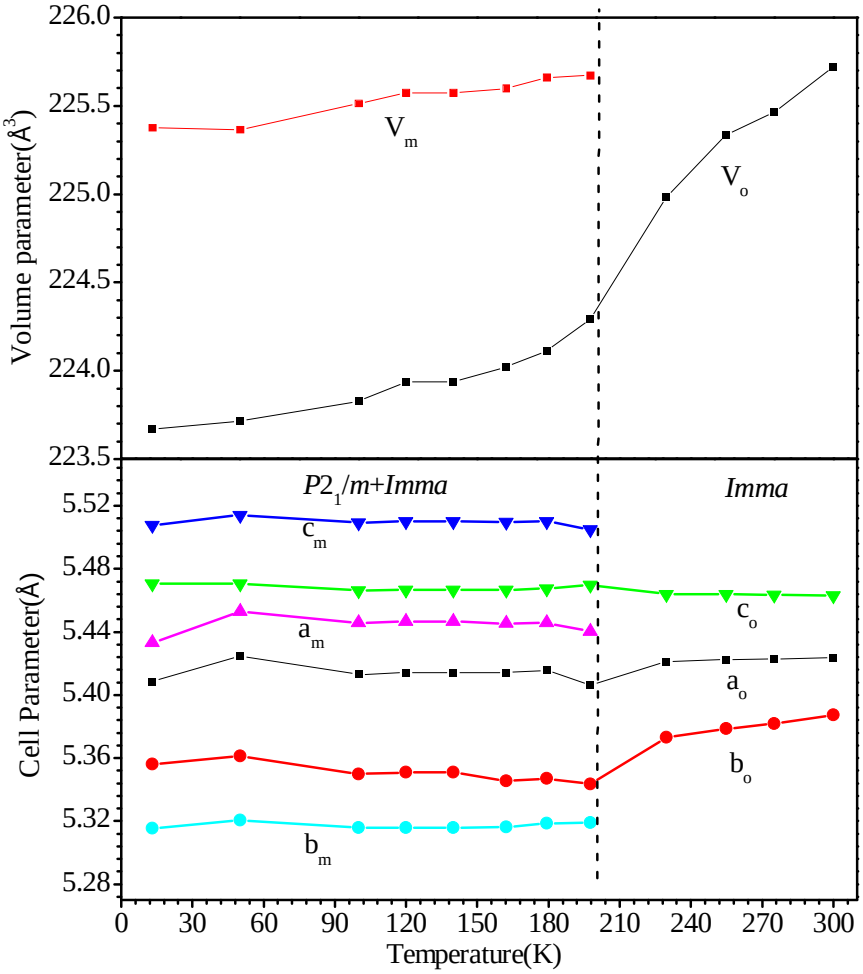

Fig. 4.10. Temperature variation of lattice parameters and unit cell volume for bulk (C13) $Nd_{0.5}Sr_{0.5}MnO_3$ obtained by Rietveld structure refinement.

The 'a_o' and 'b_o' lattice parameters of the orthorhombic phase show discontinuous change around the orthorhombic to monoclinic phase transition temperature. The unit cell volume of the monoclinic phase is nearly temperature independent at lower temperatures while that of the orthorhombic phase exhibits small thermal contraction. The unit cell volume shows discontinuous change around the orthorhombic to monoclinic phase transition suggesting first order nature of the phase transition. This is further corroborated by the wide phase coexistence region of the orthorhombic and monoclinic phases.

4.3.4 Structural Analysis of the Nanocrystalline NSMO Samples

The evolution of the selected x-ray diffraction profiles of $Nd_{0.5}Sr_{0.5}MnO_3$ samples calcined at various temperatures from 600^o C to 1300^o C is shown in Fig. 4.11. The diffraction profiles of the samples calcined at 1300 ^{o}C, 1200 ^{o}C, 1100 ^{o}C and 1000 ^{o}C are similar which suggests that the structure of these samples is orthorhombic in the Imma space group as discussed for the bulk sample in the previous section. The samples calcined at 900 ^{o}C and lower temperatures exhibit several new weak super lattice reflections which are not present in the bulk samples. These super lattice reflections are marked by letter S in Fig 4.11. The clear orthorhombic splitting of the diffraction profiles for bulk samples also disappears in the nanocrystalline samples due to crystallite size broadening leading to overlapping peaks. The presence of super lattice reflections in the nanocrystalline samples suggests that the cell size of these samples has increased by some incommensurate modulations of the unite cell parameters.

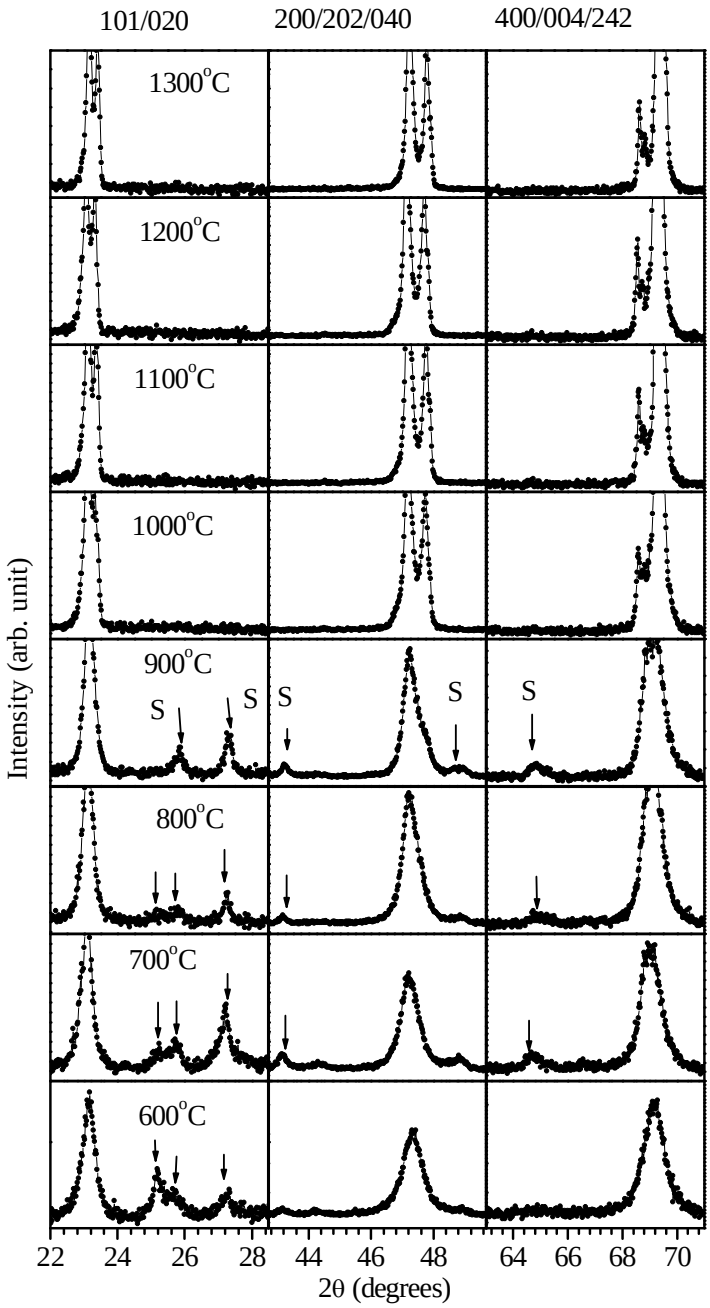

Fig. 4.11. Evolution of orthorhombic (101/020), (202/040) and (400/004/242) XRD profiles for $Nd_{0.5}Sr_{0.5}MnO_3$ samples prepared at various calcination temperatures. Miller indices on top correspond to indexing using orthorhombic structure.

Table 4.1. Rietveld structural parameters for bulk (C13) $Nd_{0.5}Sr_{0.5}MnO_3$ ceramics at room temperature using space groups *Imma*.

Imma space group at 300 K				
Atoms	x (sx)	y(sy)	z(sz)	B(Å)^2
Nd/Sr	0.0000	0.2500	-0.003 (9)	0.63 (4)
Mn	0.0000	0.0000	0.5000	1.07 (2)
O_1	0.7500	-0.015(2)	0.2500	0.37(2)
O_2	0.0000	0.2500	0.48 (1)	1.20(3)
a= 5.4307 (3)Å, b= 7.6257 (5) Å, c= 5.47117(3) Å, R_p= 15.1, R_{wp}= 19.0, R_{exp}= 12.94, χ^2=2.16				

Table 4.2. Rietveld structural parameters for bulk (C13) $Nd_{0.5}Sr_{0.5}MnO_3$ ceramics at 13K using coexisting $P2_1/m$+*Imma* space groups.

Imma space group at 13 K				
Atoms	x (sx)	y(sy)	z(sz)	B(Å)^2
Nd/Sr	0.0000	0.2500	-0.008 (2)	0.7 (1)
Mn	0.0000	0.0000	0.5000	0.2 (2)
O_1	0.7500	0.001(5)	0.2500	0.33 (8)
O_2	0.0000	0.2500	0.47 (2)	1.10(2)
a= 5.4169 (5)Å, b= 7.6308 (5) Å, c= 5.4345 (6) Å, R_p= 15.4, R_{wp}=21.1, R_{exp}= 16.68, χ^2= 1.76				
$P2_1/m$ space group at 13 K				
Atoms	X(sx)	Y(sy)	Z(sz)	B(Å)^2
Nd/Sr1	0.251 (1)	0.25000	-0.002 (2)	0.61 (1)
Nd/Sr2	0.7509 (1)	0.25000	-0.003 (2)	0.58(1)
Nd/Sr3	0.0004 (1)	0.25000	0.491(2)	0.05 (8)
Nd/Sr4	0.501 (1)	0.25000	0.5006 (2)	0.29 (8)
Mn1	0.00000	0.00000	0.00000	0.22 (1)
Mn2	0.50000	0.00000	0.00000	1.4 (1)
Mn3	0.25000	0.00000	0.491(5)	0.03(3)
O1	0.0296 (1)	0.25000	-0.0421(3)	0.049(3)
O2	0.5288 (2)	0.25000	0.026 (1)	0.039(2)
O3	0.259 (7)	0.25000	0.54 (1)	0.19(3)
O4	0.706 (6)	0.25000	0.54 (3)	0.59(1)
O5	0.108 (6)	0.022 (9)	0.254 (1)	0.79(4)
O6	0.6385 (1)	-0.031 (9)	0.24 (1)	0.39(3)
O7	0.121 (7)	-0.031 (8)	0.714 (1)	0.29(2)
O8	0.640(4)	-0.039 (6)	0.803(9)	0.19(1)
a= 10.986 (5)Å, b= 7.5092 (3) Å, c= 5.4388 (2) Å, R_p= 15.4, R_{wp}=21.1, R_{exp}= 16.68, χ^2= 1.76				

As observed for the charge ordered phase at lower temperatures in the bulk sample. To determine the structure of this modulated phase in the nanocrystalline samples various plausible structural models were considered and checked by Rietveld structure refinement.First of all we considered the orthorhombic *Pnma* space group for structure refinement and the fit is shown in Fig.4.12(b) for the C9 sample. For completeness and comparison, the fit for the *Imma* space group is also shown in Fig.4.12(a). As can be seen from Fig.4.12(b) some of the superlattice reflections are accounted by this model but many super lattice reflections are still unindexed. We then considered the low temperature $P2_1/m$ space group to refine the room temperature structure of the C9 sample calcined at 900 ^oC. As shown in Fig.4.12(c), in comparison to the *Pnma* space group, few more superlattice reflections are accounted by this space group. However, as evidenced from the difference plot there is still mismatch in the position of some of the superlattice reflections which are marked by arrow. This mismatch is more clearly seen in the fit for the XRD pattern of the sample calcined at 600 ^oC shown in Fig. 4.12(d). In view of this, we considered several other space groups like $P11m$, $P2_1nm$, $P112_1/m$, $P112_1/b$, $P2_1nb$ and $P11b$ from the subgroup of *Imma* and *Pnma* space groups to refine the structure of the nanocrystalline samples. None of the space groups could account all the superlattice reflections satisfactorily. This compels us to consider larger unit cell to explain the structure of the nanocrystalline samples. For simplicity we considered the monoclinic Pm space group in our structure refinement and introduced the modulations in a_o, b_o and c_o axes of the unit cell of the parent orthorhombic cell for bulk sample. Different combinations of the lattice modulations along a_o, b_o and c_o axes were tried to determine the correct cell size.

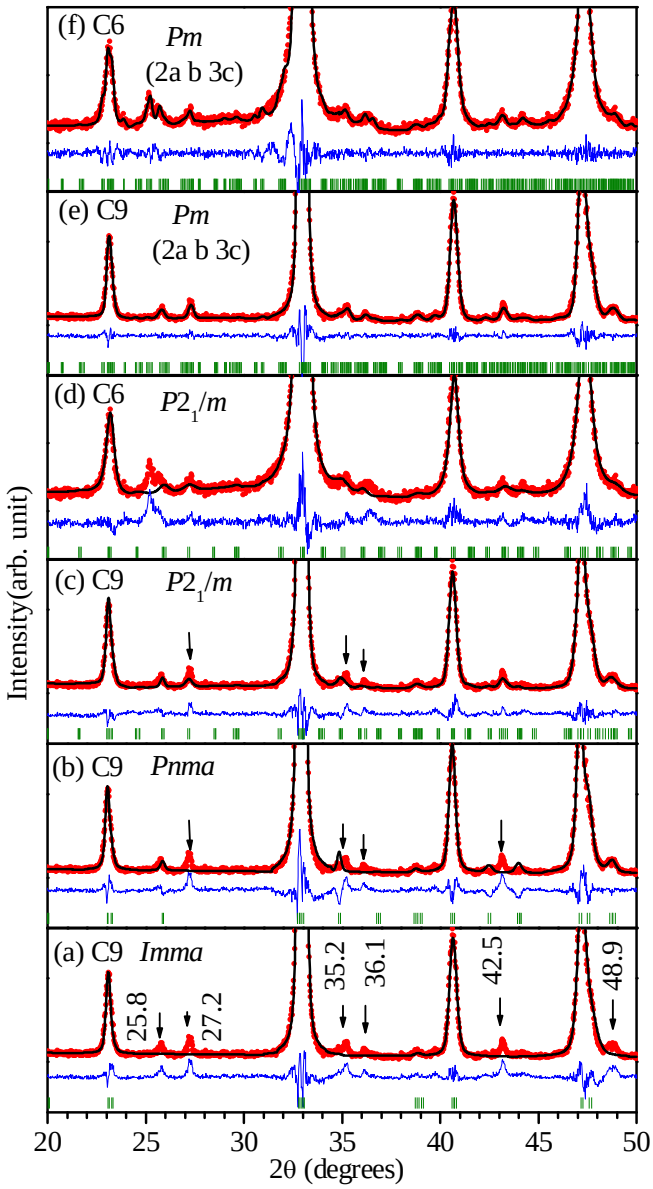

Fig. 4.12. Le-Bail profile fits for XRD patterns of nanocrystalline $Nd_{0.5}Sr_{0.5}MnO_3$ using various structural models (a) C9 sample using orthorhombic (*Imma*) (b) C9 sample using orthorhombic (*Pnma*), (c) C9 sample using monoclinic ($P2_1/m$), (d) C6 sample using monoclinic ($P2_1/m$) (e)) C9 sample using monoclinic (*Pm*) with lattice parameter ($2a_o$, b_o, $3c_o$) and (f) C6 sample using monoclinic (*Pm*) with lattice parameter ($2a_o$, b_o, $3c_o$).

After rigorous structural analysis we find that the doubling of the 'a_o' axis, keeping b_o unchanged and tripling of the 'c_o' axis satisfactorily accounts for all the superlattice reflections observed in the diffraction pattern. Very good fit between the observed and calculated XRD profiles for the C9 and C6 samples are shown in Fig.4.12(e) and (f) corresponding to this structural model. The lattice parameters obtained for modulated structure of C9 are a=10.91 Å, b=7.64 Å, and c=16.29 Å, β=90.23^o. The Rietveld fit for the complete diffraction pattern in the two theta range 15 to 120^o for C9 and C6 samples are shown in Fig.4.13. As can be seen from this figure the fit is quite good confirming our structural model for the nanocrystalline NSMO samples. A similar cell modulation and appearance of charge ordered stripes has been reported by Chen et al [Chen et al. (1997)] in $La_{0.33}Ca_{0.67}MnO_3$ using electron diffraction studies.

Variation of lattice parameters and unit cell volume with calcination temperatures for $Nd_{0.5}Sr_{0.5}MnO_3$ samples (C6-C13) are shown in Fig. 4.14. The lattice parameters of the modulated structure for the nanocrystalline samples are scaled suitably to have correspondence with the orthorhombic lattice parameters of the bulk samples. The c-parameter is nearly constant for nanocrystalline as well as bulk samples and has one to one correspondence for all the samples. There is discontinuous change in the 'a' and 'b' parameters when the transition from bulk to nanocrystalline behaviour is observed. The unit cell volume increases with decreasing calcination temperature/crystallite size for the nano samples while it slightly increases with calcination temperature/crystallite size for the bulk samples.

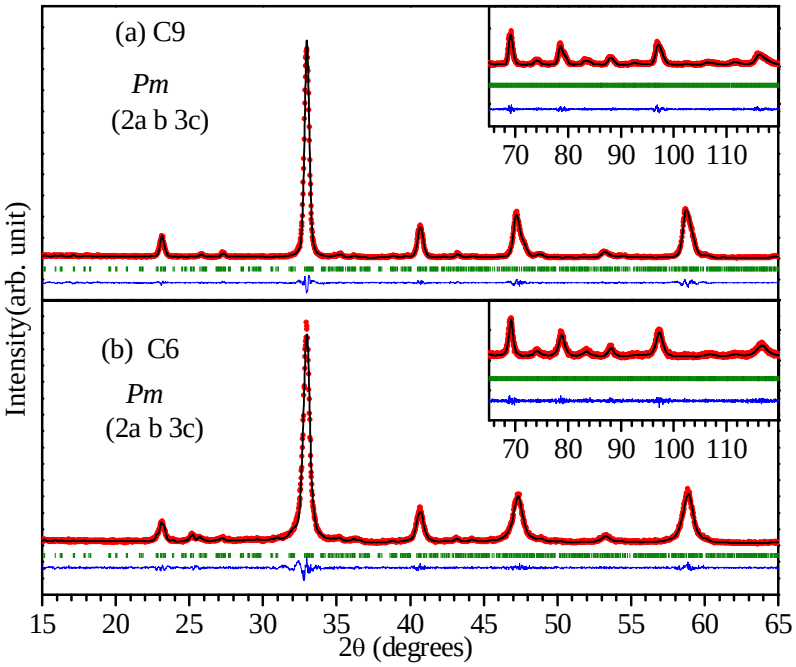

Fig. 4.13. Experimentally observed (dots), Rietveld calculated (continuous line) and their difference (continuous bottom line) profiles for nanocrystalline (a) C9 and (b) C6 $Nd_{0.5}Sr_{0.5}MnO_3$ samples obtained after Le-Bail profile matching analysis of the XRD data. The vertical tick marks above the difference plot show the Bragg peak positions.

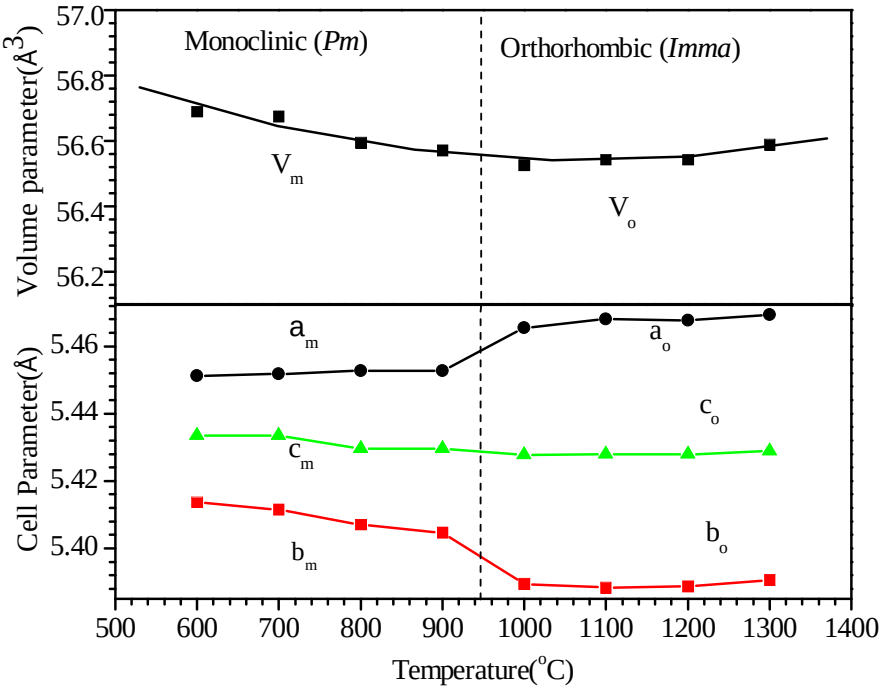

Fig. 4.14. Variation of lattice parameters and unit cell volume for nanocrystalline $Nd_{0.5}Sr_{0.5}MnO_3$ samples prepared at various calcination temperatures.

4.4 Summary

To summarize, crystal structure and magnetic behaviour of bulk and nanocrystalline $Nd_{0.5}Sr_{0.5}MnO_3$ samples of various crystallite sizes have been investigated. The nanocrystalline samples exhibit ferromagnetic behaviour and absence of charge ordering transition down to low temperatures. The Rietveld structural analysis of the nanocrystalline samples reveals that the structure can be described as a modulated phase in monoclinic structure with space group (*Pm*) which corresponds to doubled orthorhombic 'a_o' parameter and three times orthorhombic 'c_o' parameter for the structure of bulk sample at room temperature while b_o remains unchanged. The samples calcined at temperatures $\geq$1000 ^{O}C with bigger crystallite sizes exhibit bulk behavior and orthorhombic structure with *Imma* space group. The nanocrystalline samples also exhibit Griffith phase like behaviour around the paramagnetic to ferromagnetic phase transition. The bulk samples exhibits transition from room temperature orthorhombic *Imma* to monoclinic structure in the $P2_1/m$ space group at lower temperatures. For bulk samples, coexistence of the orthorhombic and monoclinic phases are observed in wide temperature range, as reported by earlier authors.